$\pi\pi$ scattering amplitudes in the subthreshold region

Gerald E. Hite
Texas A&M University at Galveston, Galveston, Texas 77553-1675

William. B. Kaufmann
Arizona State University, Tempe, Arizona 85287-1504

(Received 23 June 1997)

$\pi\pi$ scattering amplitudes inside the subthreshold triangle ($0\leqslant s\leqslant\Sigma$, $0\leqslant t\leqslant\Sigma$, $0\leqslant u\leqslant\Sigma=4\mu^2$) are studied using interior dispersion relations. The dispersion integrals are evaluated above a center-of-mass energy $W_{\pi\pi}=0.6$ GeV by using a standard phase shift analysis and from this value down to threshold by using unitary models consistent with existing low-energy experimental data. It was found that by restricting the s-wave scattering lengths to lie on a ''universal curve'' all crossing properties and appropriated threshold sum rules were reasonably well satisfied. The invariant amplitudes are found to be in good qualitative agreement with the predictions of Weinberg's chiral model and its corrections derived from chiral perturbation theory. [S0556-2813(98)04602-0]

PACS number(s): 13.75.Lb, 11.55.Bq, 11.55.Fv, 11.30.Rd

I. INTRODUCTION

The reaction $\pi\pi\rightarrow\pi\pi$ is theoretically the most elementary hadronic process [1]. The simplicity of its kinematics coupled with its beautiful crossing properties has intrigued theorists for over 30 years. In addition to its intrinsic interest, the process is an important building block in the theory of nuclear forces, neutron and proton form factors, and pion production reactions. Because of its unique role as the pseudo-Goldstone boson of chiral symmetry, chiral models [from current algebra and partially conserved axial vector current (PCAC) of the 1960s to the more recent chiral perturbation theory] are the theories of choice for understanding the low-energy dynamics of this system. These models predict the structure of the $\pi\pi$ scattering amplitude within (and somewhat beyond) the subthreshold triangle ($0\leqslant\eta\leqslant\Sigma\equiv4\mu^2$, $\eta=s,t,u$, and μ is the pion mass). It is the purpose of this article to use interior dispersion relations (IDR's) [2], experimental phase shifts, and crossing symmetry to explore the invariant amplitudes throughout the subthreshold region.

The usefulness of IDR's is due to the fact that they are written along paths (hyperbolas) which run through the physical s-channel region, the subthreshold triangle, and the physical t-channel region. If parametrizations of the experimental phase shifts are used to construct the absorptive parts of the amplitudes in the s- and t-channel dispersion integrals, then the IDR's can be used to evaluate the invariant amplitudes throughout most of the subthreshold triangle. Thus IDR's represent an excellent tool to test the predictions of chiral models provided that sufficient data exist to allow the evaluation of the dispersion integrals.

Through a series of experiments and analyses, mostly in the 1970s, phase shifts and inelasticities for $\pi\pi$ scattering have been determined indirectly through studies of pion production and kaon decay up to a center-of-mass energy of nearly $W_{\pi\pi}=2$ GeV [3–8]. Aided by the rapid convergence of our subtracted dispersion relations, these data are sufficiently accurate to allow us to perform the dispersion integrals above about 600 MeV. The low-energy $\pi\pi$ scattering amplitudes are still not precisely known, although strides have been made in that direction over the past few years [9]. By choosing scattering lengths a_{00} and a_{20} (a_{IJ}) within currently accepted bounds, we are able to find unitary parametrizations which are consistent with the sparse low-energy phase-shift data ($W_{\pi\pi}<600$ MeV) and which join onto the more abundant higher-energy data. Two different (but related) theoretical constraints are used to restrict the parameters in these fits. The first is to impose crossing symmetry, and the second is to enforce scattering-length sum rules. The results of the two methods are nearly identical and lead to an approximately linear relation between the scattering lengths a_{00} and a_{20} which closely resembles the well-known *universal curve* [10]. Our choice of IDR automatically satisfies $s\leftrightarrow u$ crossing symmetry, but $s\leftrightarrow t$ and $u\leftrightarrow t$ crossing symmetries for the calculated amplitudes are not automatic. However, for each value of a_{00} we were able, through judicious choice of a_{20}, to accommodate crossing symmetry quite satisfactorily throughout the triangle. Once the phase-shift parametrizations were chosen, we then were able to perform the dispersion integrals and, by varying the path parameter, evaluate the amplitudes throughout most of the subthreshold triangle. We conclude that the subthreshold amplitudes as revealed by the IDR analysis are in good agreement with chiral models of $\pi\pi$ scattering amplitudes. A preliminary version of this work is found in Ref. [11].

This article is organized as follows: Section II introduces the IDR's, and includes a discussion of the amplitudes, kinematics, and the paths in the Mandelstam diagram along which IDR's are written. In this section we also demonstrate that two familiar sum rules follow naturally from IDR's. Section III is devoted to the parametrization of the low-energy phase shifts through formulas that satisfy elastic unitarity and correctly describe resonance contributions. The evaluation of the dispersion relations and their comparison with chiral models are given in Sec. IV. Further discussion of interesting features of the phase-shift parametrizations is presented in an appendix.

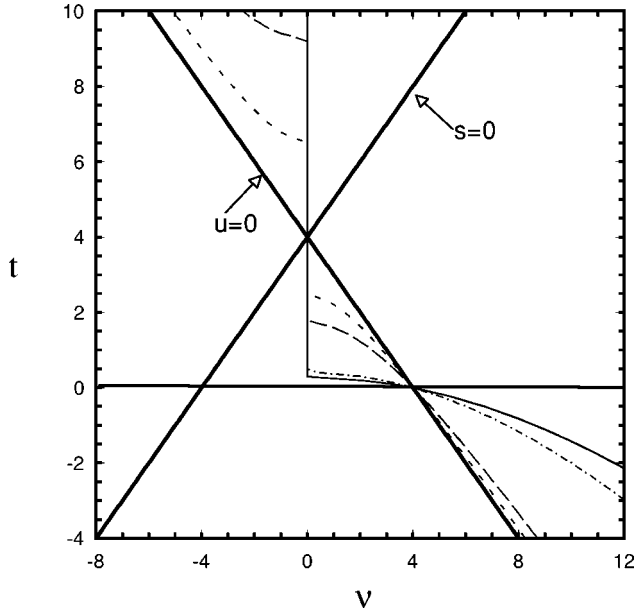

FIG. 1. Mandelstam plot for $\pi\pi$ scattering. The solid, dot-dashed, long-dashed, and short-dashed curves correspond to $a=-12.4\mu^2$, $-8\mu^2$, $-0.75\mu^2$, and $-0.25\mu^2$, respectively. The curve $a=0$ lies along the curve $u=0$. Thus for a in the region $-12.4\mu^2<a<0$ nearly all of the triangular region is accessible.

II. DISPERSION RELATIONS

A. Interior dispersion relations

Interior dispersion relations [2] can be written for amplitudes that are symmetric under $s\leftrightarrow u$ crossing. In the variables $\nu\equiv s-u$ and t, suitable amplitudes which must satisfy $A(-\nu,t)=A(\nu,t)$ can be easily constructed from the set of t-channel invariant amplitudes $A^t_{I=0,1,2}$ in which I is the isospin in the t channel. The t-channel amplitudes have partial-wave expansions

$$A^t_I=\Sigma_\ell(2\ell+1)f_{I\ell}(t)P_\ell(z_t), \tag{1}$$

$$f_{I\ell}\equiv(\eta_{I\ell}e^{2i\delta_{I\ell}}-1)/2i\rho, \tag{2}$$

where $\rho\equiv q/\sqrt{q^2+\mu^2}$, q is the t-channel center-of-mass pion momentum, and μ is the charged pion mass. Similar expressions exist for s- and u-channel amplitudes. By Bose symmetry, ℓ is even if $I=0$ or 2 and is odd if $I=1$. Under $s\leftrightarrow u$ crossing $z_t\equiv\cos\theta_t=\nu/(t-\Sigma)$ is odd, and so

$$A^t_I(\nu,t)=(-1)^I A^t_I(-\nu,t). \tag{3}$$

Consequently, su-even amplitudes suitable for IDR's are $\tilde A^t_0\equiv A^t_0$, $\tilde A^t_1\equiv A^t_1/\nu$, and $\tilde A^t_2\equiv A^t_2$, i.e., $\tilde A^t_I=A^t_I/\nu_I$, where $\nu_{0,2}=1$ and $\nu_1=\nu$.

IDR's are written by dispersing in t along curves of fixed path parameters $a=-\phi(s,t)/t^2$ where $\phi(s,t)=stu$ is the Kibble boundary function and $s+t+u=\Sigma$. Typical curves of constant path parameters are shown in Fig. 1, where they are seen to pass through both the s- and t-channel physical regions, and the subthreshold triangle. It is this latter feature that makes IDR's attractive for this work. The IDR's in their unsubtracted form are

$$\tilde A^t_I(a,t)=\frac{1}{\pi}\int_\Sigma^\infty dt'\,\frac{\tilde A^t_I(a,t')}{t'-t}+C^{st}_{I,I'}\frac{1}{\pi}\int_\Sigma^\infty ds'\,\frac{A^s_{I'}(a,t(a,s'))}{\nu'_I}\times\left(\frac{1}{s'-s}+\frac{1}{s'-u}-\frac{1}{s'-a}\right), \tag{4}$$

where $2s(a,t)=\Sigma-t+\nu$ and $2u(a,t)=\Sigma-t-\nu$ with $\nu=\nu(a,t)=\sqrt{4at+(\Sigma-t)^2}$. In the above expression the left-hand cut in t has been transformed into an integral over the physical s channel. $C^{st}_{II'}$ is the st isospin-crossing matrix [1], and a sum over I' is implied. The threshold point $s=\Sigma$, $t=0$, is common to all curves. This fact will be exploited in writing subtracted dispersion relations.

In the s-channel integral, for $a<0$ the cosine of the center-of-mass scattering angle, $z_s\equiv\cos\theta_s=(a+s')/(a-s')$, is physical, i.e., $-1<z_s<1$. In the t channel $z_t\equiv\cos\theta_t=\nu/(t'-\Sigma)$ is for $a<0$ unphysical only for t' between Σ and $t_+\equiv\Sigma-2a+\sqrt{4a(a-\Sigma)}$. In order to use partial-wave expansions of the imaginary parts of the amplitudes occurring in the integrands, it is necessary to be sure that z_t is inside the Lehmann ellipse determined by the boundary of the double spectral function ρ_{st}. In particular, one must demand that $|z_t^2|<z_{tB}^2-1$ where z_{tB} is the value of z_t at the boundary of ρ_{st}. This results in $-4a<\nu_B^2/t'$ where ν_B is the value of ν at the boundary of ρ_{st}. Using the known boundary of ρ_{st} [1], one finds the minimum value of ν_B^2/t' to be approximately 12.4Σ. Consequently, only for $-12.4\mu^2<a\leqslant 0$ is it certain that a partial-wave expansion of the amplitude in the integrand is convergent. The curve $a=-12.4\mu^2$ and others are shown in Fig. 1, and it is clear that almost all of the subthreshold triangle is accessible [12].

Subtracted IDR's are easily obtained by evaluating Eq. (4) at the s-channel threshold ($t=0$, $s=\Sigma$ for all a) and subtracting it from Eq. (4) at arbitrary t:

$$\tilde A^t_I(a,t)=\tilde A^t_I(a,0)+\frac{t}{\pi}\int_\Sigma^\infty\frac{dt'\tilde A^t_I(a,t')}{t'(t'-t)}+C^{st}_{II'}\frac{1}{\pi}\int_\Sigma^\infty ds'\,\frac{A^s_{I'}(a,t(a,s'))}{\nu'_I}\times\left(\frac{s-\Sigma}{(s'-\Sigma)(s'-s)}+\frac{u}{s'(s'-u)}\right), \tag{5}$$

where $t(a,s')=-2q^2[1-z_s(a,s')]$ and $A^t_I(a,0)=\mu C^{st}_{II'}a_{I'l=0}$. This set of equations, which is more convergent than Eq. (4), is our major tool for determining the $\pi\pi$ amplitudes within the subthreshold region.

The convergence of the dispersion integrals in Eq. (5) was first tested by comparison of its predictions along the right side of the subthreshold triangle with those of the more convergent fixed $u=0$ dispersion relation:

$$\tilde A^u_I(\nu_u)=\tilde A^u_I(\Sigma)+\frac{\nu_u^2-\Sigma^2}{\pi}\int_\Sigma^\infty\frac{d\nu'^2\tilde A^u_I(\nu'_u)}{(\nu'^2-\Sigma^2)(\nu'^2-\nu_u^2)},$$

where $\nu_u\equiv s-t$. The tilde represents division by ν_{uI}, so that these amplitudes are even under st crossing. This dispersion

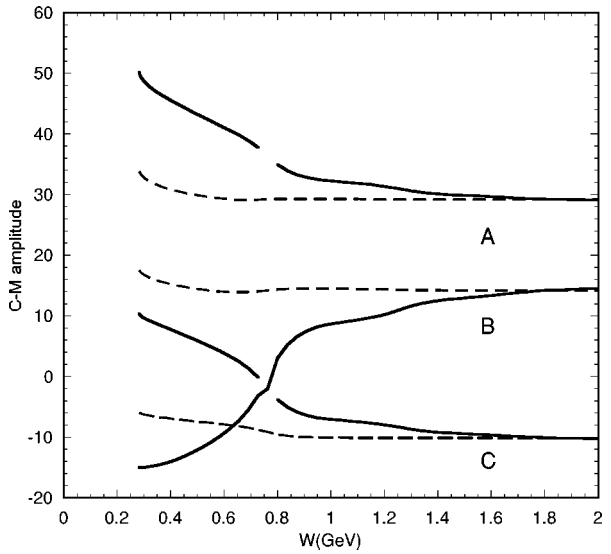

FIG. 2. Convergence of the dispersion integrals. Both s- and t-channel integrals were truncated at a center-of-mass energy W. The value at the left side of each graph corresponds to setting the dispersion integrals to zero, the value at the right, the integral up to $W=2$ GeV. (a) shows the W dependence of the subtracted IDR, (b) that of the fixed-u dispersion relation. Although the latter has better convergence properties, both are seen to converge to the same values. For this particular example $t=2.16\mu^2$ and $\nu=1.04\mu^2$, but the results are typical for other points within the triangle.

relation has been subtracted at the s-channel threshold, $\nu_u=\Sigma$, resulting in $\tilde{A}_I^u(\Sigma)=\mu C_{II'}^{su}a_{I'l=0}/\Sigma_I$. By comparing this integral to that of the once-subtracted IDR, it is seen that this integrand has an extra energy-squared factor to speed convergence. Once the amplitudes on the line $u=0$ were determined, their values within the interior of the triangle were found from strongly convergent dispersion relations obtained by subtracting Eq. (5) with general a from a similar expression with $a=0$ and the same value of t, the subtraction constant $\tilde{A}_I^t(0,t)$ being obtained from $\tilde{A}_I^u(\nu_u)$ of Eq. (6) by applications of the tu crossing matrix.

Figure 2 compares the convergence of these two methods by showing the accumulative integrals for the Chew-Mandelstam amplitudes as functions of the cutoff energy W, i.e., the highest center-of-mass energy included in the integrals. In all cases, we have found convergence in the doubly subtracted method well below $W=2.0$ GeV, the highest energy for which experimental phase shifts are available (see Sec. III). The convergence is poorer, but still satisfactory for evaulations using Eq. (5). The two methods yield nearly equal amplitudes, providing a good consistency check, because they weigh the regions of integrations differently.

B. Threshold sum rules

IDR's simplify to boundary dispersion relations [13] when they are evaluated at path parameters $a=0$ where $z_s=z_t=-1$. By its definition, $\tilde{A}_1^t$ includes an additional factor of $\nu^{-1}=(\Sigma-t)^{-1}$, and thus its integrals converge as if they were subtracted. In its unsubtracted form, it can be written as

$$A_1^t(0,t)/\nu=\frac{1}{\pi}\Sigma_\ell(2\ell+1)\left[\int_\Sigma^\infty\frac{dt' f_{1\ell}(t')}{(t'-t)(t'-\Sigma)}+(-1)^I C_{1I}^{st}\int_\Sigma^\infty\frac{ds' f_{I\ell}(s')}{s'(s'-\nu)}\right]. \quad (6)$$

This amplitude can be evaluated at $t=\Sigma$, $\nu=0$ to obtain the Olsson sum rule or at $t=0$, $\nu=\Sigma$ to obtain the sum rule involving $2a_{00}-5a_{20}$; see Ref. [1], p. 262. Doing this and changing the integration variable to ρ yields

$$3a_{11}\mu^3=\frac{2}{\pi}\Sigma_\ell(2\ell+1)\int_0^1 d\rho(\rho^{-3}f_{1\ell}-\rho C_{1I}^{su}f_{I\ell}) \quad (7)$$

and

$$\frac{2a_{00}-5a_{20}}{6}\mu=\frac{2}{\pi}\Sigma_\ell(2l+1)C_{1I}^{st}\int_0^1\frac{d\rho}{\rho}f_{I\ell}, \quad (8)$$

respectively. Subtracting these two sum rules yields

$$\frac{1}{6}(18a_{11}\mu^2-2a_{00}+5a_{20})\mu$$

$$=\frac{2}{\pi}\Sigma_\ell(2\ell+1)\int_0^1\frac{d\rho(1-\rho^2)}{\rho^3}(f_{1\ell}-C_{1I}^{su}\rho^2 f_{I\ell}). \quad (9)$$

The factor of $(1-\rho^2)$ in the last integral ''pinches off'' the high-energy contributions, leading to improved convergence. This sum rule is equivalent to one first proposed by Wanders [14]. This combination of scattering lengths vanishes in Weinberg's chiral model [15], and so it is expected to be quite small.

III. PARAMETRIZATION OF $\pi\pi$ PARTIAL-WAVE AMPLITUDES

To evaluate the dispersion integrals, it is necessary to have parametrizations of partial-wave amplitudes (PWA's) for each isospin state. For the low-energy region ($W=\sqrt{s}<0.6$ GeV or $\rho<0.93$), we will use parametrizations for the s- and p-wave amplitudes that correctly describe resonance contributions: They have resonance poles on the unphysical sheet, have correct threshold behavior, and are real below threshold. As shown in the Appendix these parametrizations can be used to generate solutions of partial-wave dispersion relations and form factors. In the region above approximately 0.6 GeV and for d and f waves, we use the parametrization of Hyams *et al.* [6].

Effective-range parametrizations of PWA's normally are written as expansions of the form $q^{2\ell+1}\cot\delta_\ell(q)=\Sigma_\ell c_\ell q^{2\ell}$ where the series is truncated at a convenient point. For low-energy $\pi\pi$ scattering, we replace q in this expression by the variable ρ. The variable ρ is a natural variable in which to write resonance parametrizations that satisfy elastic unitarity and also, as seen in the previous section, to write dispersion relations. We will begin by listing simple parametrizations for the first few PWA's.

A. *s*-wave partial-wave amplitudes

Defining $f_0 \equiv t_0/\rho \equiv (S_0-1)/2i\rho$, in the elastic region it follows that

$$f_0^{-1} = -i\rho + \rho\cot\delta_0 \tag{10}$$

(isospin labels are omitted). Keeping the first three terms of an effective-range expansion gives

$$\rho\cot\delta_0^{(2)} = c_0 + c_2\rho^2 + c_4\rho^4, \tag{11}$$

where the constants c_0, c_2, and c_4 are real. The constant c_0 is the inverse of the scattering length a_0 in pion mass units, and c_2 is twice the ''effective-range'' parameter for an expansion in ρ^2. This parametrization can give good fits to experimental data for a reasonable range of $c_0 = 1/\mu a_0$. Substituting Eq. (11) into Eq. (10) results in a polynomial in ρ whose roots are poles of the PWA's. Resonance poles are the ones which correspond to ρ in the interval (0,1) with small negative ρ. The model of Eq. (11) does not describe two resonances; the right-hand side is finite, and hence the phase shift cannot pass through π. Once the parameters c_i are found by fitting phase-shift data, the roots of f_0^{-1} can be found and the appropriate one inverted via $s = \Sigma/(1-\rho^2) = M^2 - iM\Gamma$ to give the mass and width of the resonance.

Although it will not be required in the low-energy regime, where the previous fits are adequate, we could obtain an appropriate expression for two resonances (or two bound states) by use of the well-known, crude, but unitary, model $S_{2r} = S_{r_1}S_{r_2}$, where $S_{r_i} = 1 + 2i\rho f_{r_i}$, to obtain

$$f_{2r}^{-1} = -i\rho + \frac{(c_{10}+c_{12}\rho^2)(c_{20}+c_{22}\rho^2) - \rho^2}{c_{10}+c_{20}+(c_{12}+c_{22})\rho^2}, \tag{12}$$

where $f_{r_i}^{-1} = -i\rho + c_{i0} + c_{i2}\rho^2$. A change of parameters may be made to yield

$$f_{2r}^{-1} = -i\rho + (\mu a_0)^{-1}(1-\rho^2/\rho_{\pi/2}^2) \times (1-\rho^2/\rho_{3\pi/2}^2)/(1-\rho^2/\rho_\pi^2). \tag{13}$$

For some values of the parameters c_{ij} (e.g., for two resonances) the constants $\rho_{\pi/2}$, ρ_π, and $\rho_{3\pi/2}$ are real. This form clearly illustrates the pole and zeros of $\rho\cot\delta = f^{-1} - i\rho$ at $\delta = \pi$ and $\delta = \pi/2$, $3\pi/2$, respectively. Once the four parameters are found by fitting phase-shift data, the roots of $(1-\rho^2/\rho_\pi^2)f_{2r}^{-1}$ can be found as before to give the masses and widths of the two resonances. The procedure is easily extended to include additional resonances.

1. δ_{00}

For $I=0$ amplitudes we have adopted the phase-shift analysis of Estabrooks and Martin [5] for the higher-energy data and that of Rosselet *et al.* [7] for the lower-energy data. The data of Rosselet *et al.* (below $\rho^2 = 0.5$) have relatively large error bars, and so do not strongly constrain the fit in the low-energy region. A parametrization of the form

$$\rho\cot\delta_{00}^{(3)} = \frac{1}{\mu a_{00}} + c_2\rho^2 + c_4\rho^4 \tag{14}$$

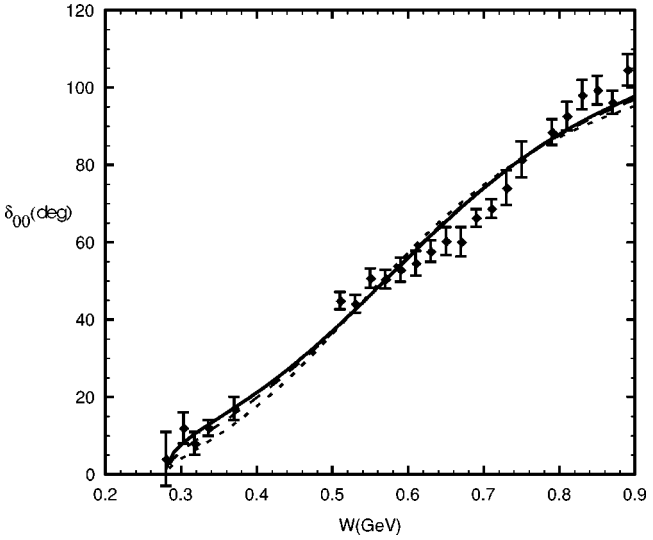

FIG. 3. *s*-wave isospin-0 phase shift δ_{00} vs $W_{\pi\pi}$. Experimental phase shifts are from Refs. [5] and [7]. The three fits correspond to $\mu a_{00} = 0.16$ (short-dashed line), 0.26 (long-dashed line), and 0.36 (solid line).

was fit to data below 0.9 GeV with a_{00} as an input parameter. The best-fit parameters for each choice of a_{00} were found to vary linearly in a_{00}^{-1}: $c_2 = 7.14 - 2.56(\mu a_{00})^{-1}$, $c_4 = -8.10 + 1.62(\mu a_{00})^{-1}$ for $0.10 < \mu a_{00} < 0.35$. (The coefficients are given to three places to allow the reader to reproduce our numbers.) This parametrization has a ''sigma meson'' with mass in the general region of 0.5 GeV and width of 0.7 GeV for a broad range of a_{00}. The fit is shown in Fig. 3. Deviations from the data that begin near $W = 0.9$ GeV are irrelevant as it is used only below 0.60 GeV.

To test the dependence of the effective-range parameters on the data set used to model the phase shift between 0.6 GeV and 0.9 GeV, we have also obtained values of c_2 and c_4 by replacing the low-energy data of Ref. [5] by those of two others, with the following results: Ref. [8], $c_2 = 5.08 - 2.58(\mu a_{00})^{-1}$, $c_4 = -5.80 + 1.64(\mu a_{00})^{-1}$; Ref. [6], $c_2 = 6.28 - 2.52(\mu a_{00})^{-1}$, $c_4 = -7.00 + 1.57(\mu a_{00})^{-1}$. This should give some indication of the uncertainty of these parameters.

In all of our parametrizations, the predicted mass and widths of the ''sigma meson'' are fairly consistent. Törnqvist and Roos have recently advocated the interpretation of σ as a real, physical particle [16], and the resilience of the pole position of our fits for several (admittedly simple) parametrizations is in agreement with their view.

2. δ_{20}

To allow a variation of a_{20} as used in the dispersion work in the next section, a parametrization of the form $\rho\cot\delta_{20} = (\mu a_{20})^{-1} + c_2\rho^2 + c_4\rho^4$ was fit to the data of Hoogland *et al.* [4] for $-0.20 < \mu a_{20} < -0.02$. As functions of the scattering length, the best-fit parameters were found to be $c_2 = -22.62 - 2.41(\mu a_{20})^{-1}$ and $c_4 = 21.64 + 1.43(\mu a_{20})^{-1}$. Corresponding curves and the data are shown in Fig. 4. These fits are used only for $W < 0.6$ GeV.

B. *p*-wave partial-wave amplitude δ_{11}

For $l=1$, the reduced PWA $h_{11} \equiv (S_{11}-1)/2i\rho^3$ could be parametrized in the elastic region by using $\rho^3\cot\delta_{11}$

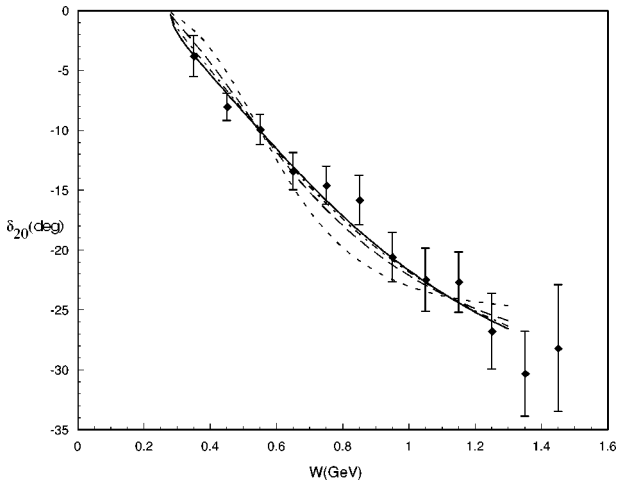

FIG. 4. s-wave isospin-2 phase shift δ_{20} vs $W_{\pi\pi}$. Experimental phase shifts are from Ref. [4]. The four fits correspond to $\mu a_{20}=-0.02$ (short-dashed line), -0.04 (long-dashed line), -0.06 (dot-dashed line), and -0.08 (solid line).

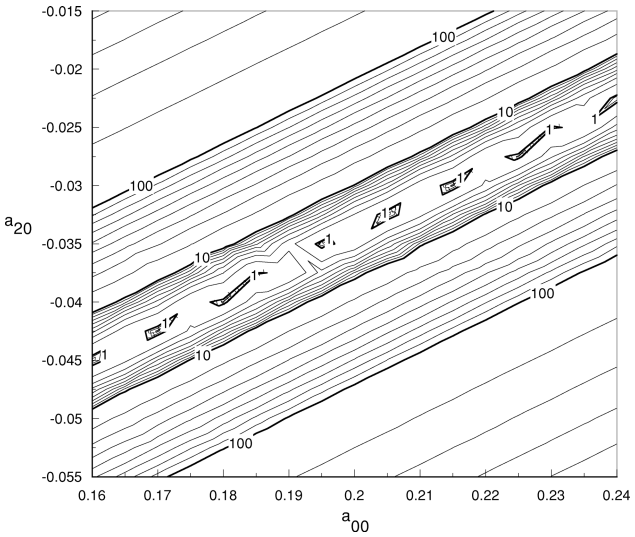

FIG. 5. ''Universal curve.'' The relation between a_{00} and a_{20} which produces acceptable crossing symmetry. The contours correspond to lines of constant 10^4X. The jitter at the bottom of the trough is an artifact of the grid spacing.

$=(\mu^3 a_{11})^{-1}+c_2\rho^2=(1-\rho^2/\rho_{\pi/2}^2)/(\mu^3 a_{11})$. Fitting this to the phase shifts of [5] results in the resonance poles $-\rho_\rho^*$ and $\rho_\rho=0.931-0.014i$ and a distant satellite pole at $\rho_s=31.67i$. The mass and width of the resonance pole are $M_\rho=751$ MeV and $\Gamma_\rho=144$ MeV. The scattering volume for this fit is $\mu^3 a_{11}=0.036$.

To describe the contribution of two resonances where the phase can vary from zero to 2π, a better parametrization would be

$$\rho^3\cot\delta_{11}^{(2r)}=(\mu^3 a_{11})^{-1}(1-\rho^2/\rho_{\pi/2}^2)\times(1-\rho^2/\rho_{3\pi/2}^2)/(1-\rho^2/\rho_\pi^2). \quad (15)$$

Once the parameters are found from fitting data, the masses and widths of the resonances can be found from the roots of $h_{11}^{-1}(\rho)=-i\rho^3+\rho^3\cot\delta_{11}$.

IV. $\pi\pi$ SCATTERING AMPLITUDES IN THE SUBTHRESHOLD TRIANGLE

A. Crossing, sum rules, and a universal curve

The next step is to insert the imaginary parts of the partial-wave amplitudes into the subtracted IDR, Eq. (5), to evaluate the amplitudes A_I^t inside the subthreshold triangle. For each choice of s-wave scattering lengths, we evaluated them at a fine grid of points (ν,t) within the subthreshold triangle as described below. With this set of amplitudes, we were able to test the crossing symmetry.

The crossing properties of the $\pi\pi$ scattering amplitude are most simply and elegantly expressed in terms of the invariant amplitudes of Chew and Mandelstam (CM) [17], which are defined by $T(s,t,u)=\delta_{\alpha\beta}\delta_{\gamma\delta}A(s,t,u)+\delta_{\alpha\gamma}\delta_{\beta\delta}B(s,t,u)+\delta_{\alpha\delta}\delta_{\beta\gamma}C(s,t,u)$ in terms of Cartesian isospin indices. The crossing properties of the CM amplitudes are summarized as follows: under $s\leftrightarrow u$, $A(s,t,u)=C(u,t,s)$ and $B(s,t,u)=B(u,t,s)$; under $s\leftrightarrow t$, $A(s,t,u)=B(t,s,u)$ and $C(s,t,u)=C(t,s,u)$; and under $t\leftrightarrow u$, $A(s,t,u)=A(s,u,t)$ and $B(s,t,u)=C(s,u,t)$. The CM amplitudes are related to the t-channel invariant amplitudes, by $A_0^t=3B+A+C$, $A_1^t=A-C$, and $A_2^t=A+C$. Inverting these equations, we can determine A, B, and C in terms of the A_I^t's, which were previously calculated within the subthreshold triangle.

Because the t-channel invariant amplitudes obey $A_I^t(\nu,t)=(-1)^I A_I^t(-\nu,t)$ [see Eq. (3)] under $s\leftrightarrow u$ (i.e., $\nu\rightarrow-\nu$), it follows immediately that the resulting CM amplitudes exactly satisfy the desired su crossing properties. On the other hand, we have no assurance that the amplitudes generated from the IDR's will possess the correct crossing properties under the permutations $s\leftrightarrow t$ and $t\leftrightarrow u$, and in general they do not. If, for example, typical values $a_{00}\mu=0.20$ and $a_{20}\mu=-0.10$ of the s-wave scattering lengths are chosen, the $s\leftrightarrow t$ relations are poorly satisfied. However, a rather small modification of either scattering length can produce amplitudes which do possess to a reasonable approximation the desired crossing properties for pairs of points related by $s\leftrightarrow t$ crossing. Consequently, to ensure a rather accurate crossing symmetry within the subthreshold triangle, we chose a uniform grid of points within the subthreshold triangle (''uniform'' means equal spacing in the Dalitz variables x and y where $\nu=\sqrt{3}x$ and $t=y$). Points for which $a<-8\mu^2$ are eliminated so that the partial-wave expansions of the t-channel amplitudes lie well within their ellipses of convergence, as was discussed in Sec. II A. For the set of such points $c=(\nu,t)=(s,t,u)$ we form the sum of the squares of the difference of the CM amplitudes at $s\leftrightarrow t$ crossing symmetric points throughout the right-hand half $(\nu>0)$ of the subthreshold triangle (e.g., all terms such as $[A(s,t,u)-B(t,s,u)]^2$ and $[C(s,t,u)-C(t,s,u)]^2$, etc.). Using the automatic $s\leftrightarrow u$ crossing properties of the amplitudes this sum can be written as $X=\Sigma_c X_c$, where

$$X_c\equiv(A_b-A_c)^2+(B_b-C_c)^2+(C_b-B_c)^2+(A_d-C_c)^2+(B_d-A_c)^2+(C_d-B_c)^2+(A_d-B_b)^2+(B_d-A_b)^2+(C_d-C_b)^2, \quad (16)$$

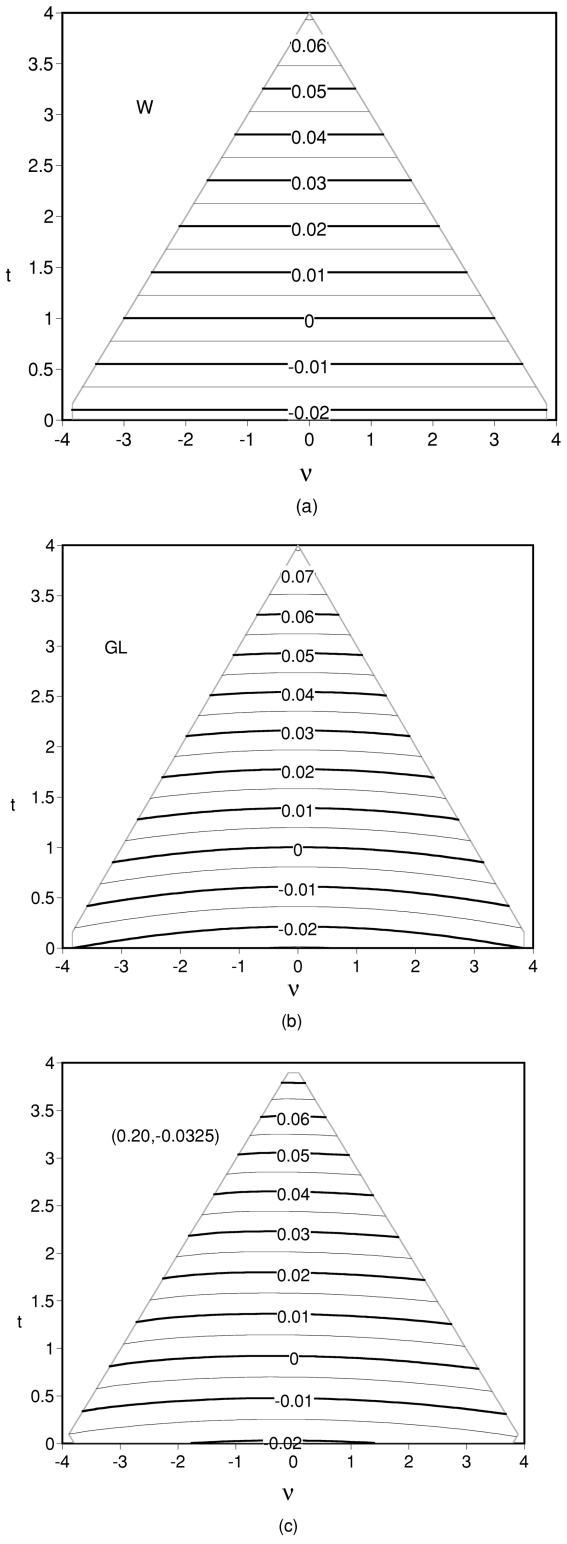

FIG. 6. Contours of $B(s,t,u)$ throughout the subthreshold triangle. (a), (b), and (c) correspond to the Weinberg amplitude (W), the amplitude of Gasser and Leutwyler (GL), and the IDR result for the case $\mu a_{00}=0.20$, $\mu a_{20}=-0.0325$.

$d=(u,s,t)$, $b=(s,u,t)$, and c is restricted to lie in the smaller triangle bounded by $t=0$, $u=t$ and $s=u$. The same expression results from summing over $u\leftrightarrow t$ crossing symmetric points. By construction, X vanishes for a fully crossing-symmetric set of CM amplitudes. For each value of

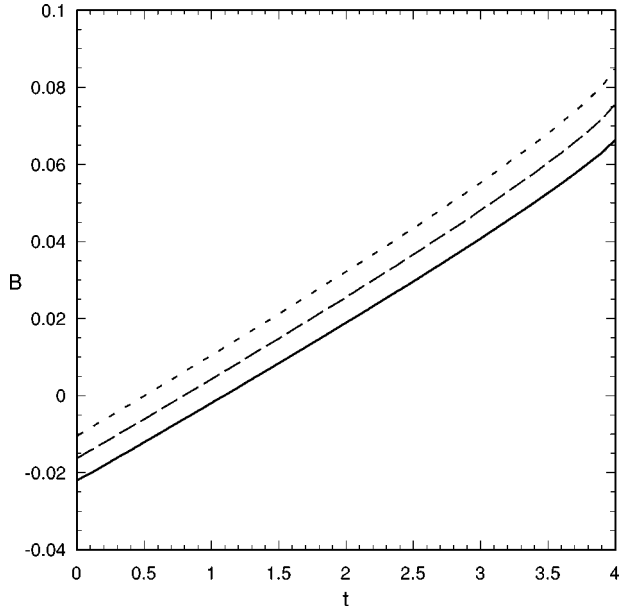

FIG. 7. B amplitude along the line $u=0$: $B(t)=B(\Sigma-t,t,0)$. The three curves correspond to scattering lengths $\mu a_{00}=0.16$ (solid line), 0.20 (long-dashed line), and 0.24 (short-dashed line).

a_{00}, we have selected the value of a_{20} which best minimizes X. A plot of X as a function of a_{00} and a_{20} is given in Fig. 5. The points preferred by crossing symmetry lie on the deep trough seen in the figure. The values of a_{00} and a_{20} found in this manner lie roughly along the ''universal line''

$$a_{20}=-0.090\mu^{-1}+0.288a_{00}. \tag{17}$$

This equation differs slightly from the result we presented in Ref. [11] because an earlier version of the partial waves of Estabrooks *et al.* was used in that work and crossing symmetry was enforced on a more limited grid. If a fit to a combination of the data of Rosselet *et al.* and the 15 lowest-energy points of the data Hyams *et al.*, the result is

$$a_{20}=-0.089\mu^{-1}+0.275a_{00}, \tag{18}$$

in reasonable agreement with Eq. (17). A measure of the excellent quality of crossing symmetry compliance is $\sqrt{X/9N}\approx 0.0002$, where N is the number of sample points, usually taken to be 330, and 9 is included because there are nine terms in X. This number is to be compared with the sizes of the CM amplitudes, which lie approximately within the interval $(-0.02,0.08)$.

Next we test the consistency of the points on the ''universal'' curve with the sum rules, Eqs. (7) and (8) found in Sec. II B. The sum rules were evaluated through the parametrizations discussed in Sec. III. As an example we take $a_{00}=0.20\mu^{-1}$; the corresponding value of a_{20} chosen from the ''universal curve'' is $a_{20}=-0.0325\mu^{-1}$. The left-hand side of Eq. (8) yields $2a_{00}-5a_{20}=0.56\mu^{-1}$ while evaluating the right-hand side from the phase shifts yields $0.55\mu^{-1}$. With this choice of scattering lengths then there is reasonable consistency. Using the same choice of parametrization Eq. (7) yields $a_{11}=0.033\mu^{-3}$. The effective-range formula (Sec. III B) used to model the low-energy p waves gives $0.036\mu^{-3}$. The right-hand side of the Wanders sum rule, Eq.

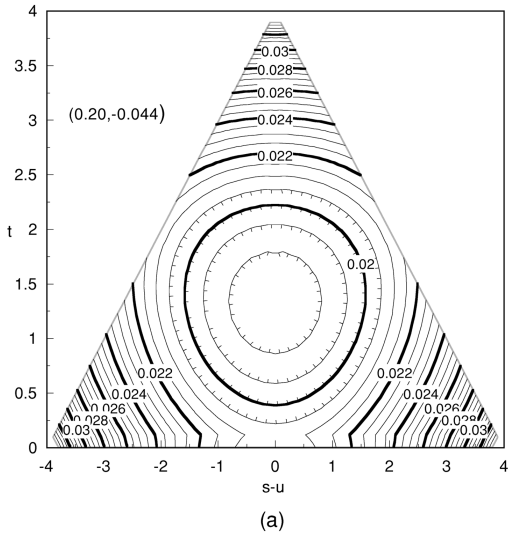

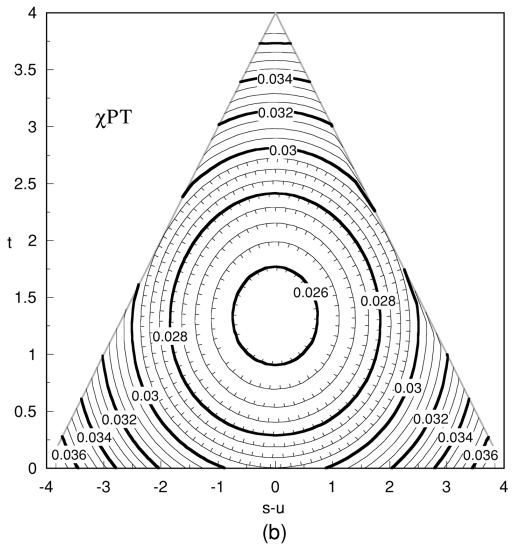

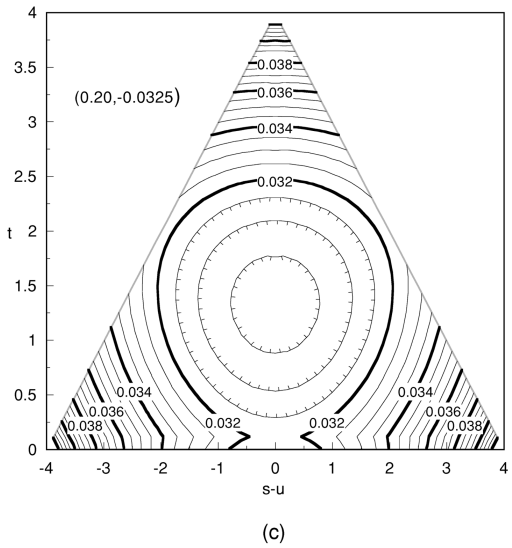

FIG. 8. Contours of $A+B+C$ corresponding to $\pi^0\pi^0$ elastic scattering. (a) and (c) correspond to two IDR calculations corresponding to two different fits to the low-energy data (kinks at bottom are artifacts), and (b) corresponds to the amplitude of Gasser and Leutwyler. Weinberg's amplitude is a constant (approximately 0.022) everywhere.

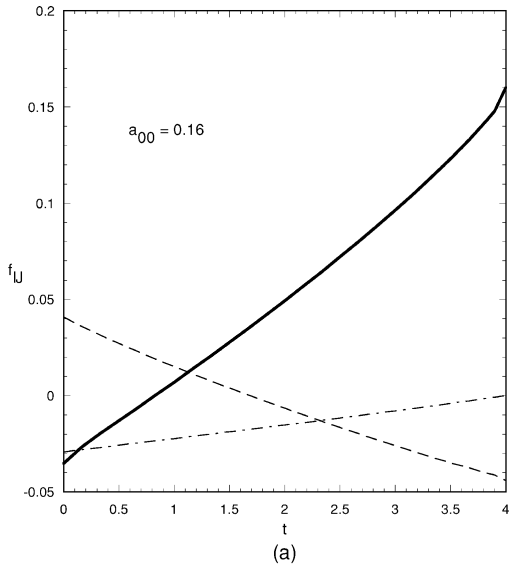

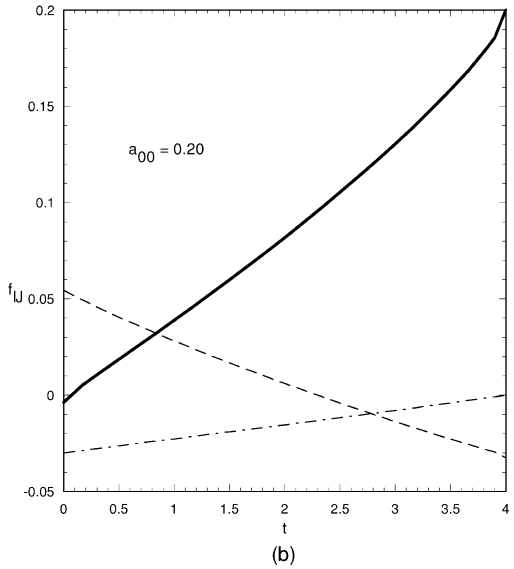

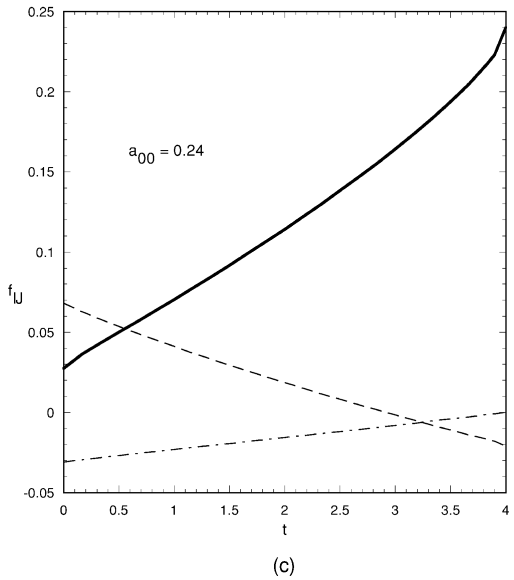

FIG. 9. Partial-wave amplitudes. f_{00}, f_{11}, and f_{20} correspond to solid, dot-dashed, and dashed lines. (a), (b), and (c) correspond to $\mu a_{00}=0.16$, 0.20, and 0.24, respectively.

(9), yields $(2a_{00}-5a_{20})\mu-18a_{11}\mu^3=0.554-0.589=-0.035$, and so, as expected, the cancellation between the two contributions is quite strong.

B. Comparison to models with chiral symmetry

The study of low-energy pion processes leads naturally to the realization that chiral symmetry is a good approximate symmetry of strong interactions. Low-energy $\pi\pi$ scattering is an especially attractive process for testing chiral-symmetry-breaking models. As early as 1966 Weinberg [15], employing current algebra and PCAC, derived the following approximate expression the CM amplitude B:

$$B(s,t,u)=(t-\mu^2)/(16\pi f_\pi^2), \tag{19}$$

where $f_\pi\approx 93\sqrt{2}$ MeV is the pion decay constant. Corresponding expressions for the amplitudes A and C are found by replacing t by s and u, respectively. This amplitude has three distinct features: (a) It is a linear function of t alone, (b) its slope is $1/(16\pi f_\pi^2)$, and (c) it has a null line at $t=\mu^2$. More recently, corrections to Weinberg's amplitude have been derived within the framework of chiral perturbation theory [18–21]. These corrections produce slight nonlinearities in the amplitudes which are interesting to compare with our results.

As was seen in Sec. IV A, the amplitude B can be constructed from the t-channel isospin amplitudes, i.e., $(A_0^t-A_2^t)/3$, which have been evaluated via the dispersion relations inside the subthreshold triangle. Figure 6 compares our contour plot of B [Fig. 6(c)] with the chiral amplitudes of Weinberg [Fig. 6(a)] and of Gasser and Leutwyler [Fig. 6(b)]. In our calculation we have used the case $(a_{00},a_{20})\mu=(0.20,-0.0325)$ which lies on the universal curve Eq. (17). The similarity of our contours to those predicted by Weinberg's model is evident. Closer inspection shows, however, that the contours are slightly bowed, implying a s^2+u^2 or higher dependence, and are not equally spaced, implying a t^2 or higher dependence qualitatively similar to the higher-order corrections of Refs. [18,19].

As Fig. 7 shows more clearly, $B(s=\Sigma-t,t,u=0)$, (a) is nearly linear in t, (b) has a slope on the order of $1/(16\pi f_\pi^2)$, and (c) has a null line at $t\approx\mu^2$ for $a_{00}\approx 0.20\mu^{-1}$. The figure also indicates that, to lowest order, variation of a_{00} translates the curves slightly in t.

A more sensitive test of the corrections to Weinberg's amplitude is provided by $\pi^0\pi^0$ elastic scattering, for which the amplitude is $A+B+C$. This amplitude is symmetric under any permutation of s, t, and u. Weinberg's amplitude for this process is the constant $\mu^2/16\pi f_\pi^2\approx 0.022$, and so deviations from constancy are a direct measure of the correction terms. Figure 8 compares the results of the chirally corrected amplitude [19] with our result. The figure also includes a contour plot using an effective-range formula fit to the data of [8] to show an indication of the our uncertainties. The values of a_{20} are different because the ''universal'' lines, imposed by crossing symmetry, are slightly different for the two fits. All three plots show a minimum at the symmetry point $s=t=u=4\mu^2/3$, in accordance with a rigorous theorem of A. Martin [22].

As another example, Knecht *et al.* [20] by including one-loop graphs in ''generalized chiral perturbation theory'' obtain

$$\begin{aligned}16\pi B(s,t,u)=&\left[\beta\left(t-\frac{4}{3}\mu^2\right)+\frac{1}{3}\alpha\mu^2\right]\Big/\ f_\pi^2+[\lambda_1(t-2\mu^2)^2+\lambda_2(s-2\mu^2)^2+\lambda_2(u-2\mu^2)^2]/f_\pi^4\\&+\overline{J}(s)\left\{8\left[\beta\left(t-\frac{4}{3}\mu^2\right)+\frac{5}{6}\alpha\mu^2\right]^2-2\left[\beta\left(t-\frac{4}{3}\mu^2\right)-\frac{2}{3}\alpha\mu^2\right]^2\right\}\Big/\ (12f_\pi^4)\\&+\overline{J}(t)\left\{3\left[\beta\left(s-\frac{4}{3}\mu^2\right)-\frac{2}{3}\alpha\mu^2\right]^2+\beta^2(t-u)(t-4\mu^2)\right\}\Big/\ (12f_\pi^4)\\&+\overline{J}(u)\left\{3\left[\beta\left(u-\frac{4}{3}\mu^2\right)-\frac{2}{3}\alpha\mu^2\right]^2+\beta^2(t-s)(u-4\mu^2)\right\}\Big/\ (12f_\pi^4),\end{aligned}$$

where $\overline{J}(s)\equiv[1-\rho Q_0(\rho)]/8\pi^2$ and Q_0 is the zeroth-order Legendre function of the second kind, i.e.,

$$Q_0(\rho)=\frac{1}{2}\left[\ln\left(\frac{1+\rho}{1-\rho}\right)-i\pi\right]$$

since $\rho\geq 0$.

The first term dominates and, for $\alpha=\beta=1$, reproduces Weinberg's result. Values of the four parameters $(\alpha,\beta,\lambda_1,\lambda_2)$ can be found for which the contours for this model are indistinguishable from those shown in Fig. 6(c). The parameter sets corresponding to three typical scattering lengths are $[a_{00}\mu=0.16$: $(0.409,0.938,-0.0036,0.0115)]$, $[a_{00}\mu=0.20$: $(1.246,0.947,-0.0036,0.0117)]$, and $[a_{00}\mu=0.24$: $(2.068,0.953,-0.0039,0.0118)]$. These may be compared with the results of Knecht *et al.* [21], who give $\lambda_1=(-6.4\pm 6.8)\times 10^{-3}$, $\lambda_2=(10.8\pm 1.2)\times 10^{-3}$, $\alpha=2.6$, and $\beta=1.19$ as representative values.

C. Comparison of partial-wave amplitudes

Pennington and Protopopescu [23] used the Roy equations [24] to evaluate the lowest partial waves in each of the three isospin channels in the subthreshold region. We have

performed a partial-wave projection of our evaluation of the full subthreshold amplitudes for comparison with their results. Our results are plotted in Fig. 9 and are in reasonable agreement with Ref. [23] for the case $(a_{00},a_{20})\mu=(0.16, -0.044)$. We also present the cases for which $a_{00}\mu=0.20$ and 0.24. For the first case f_{00} and f_{20} have zeros at approximately $t\approx 0.7\mu^2$ and $2.4\mu^2$, respectively. The corresponding points in the model of Weinberg are $0.5\mu^2$ and $2.0\mu^2$. $f_{00}(t)$ has a steep positive slope which leads to large $I=J=0$ amplitudes at a few hundred MeV even though the scattering length is itself rather small. $f_{20}(t)$ has a shallower negative slope. The expansions of the partial-wave amplitudes in powers of q_t^2 are $\mathrm{Re}f_{I0}(t)\mu^{-1}=a_{I0}+b_{I0}q_t^2+\cdots$ near the t-channel threshold, where a_{I0} are the scattering lengths and b_{I0} are the slope parameters. The results corresponding to Fig. 9(a) are $b_{00}=0.29\mu^{-3}$ and $b_{20}=-0.07\mu^{-3}$. The scattering volume for the p wave is given by $\mu^3 a_{11}=\lim_{\rho\to 0}\rho^{-2}f_{11}=0.033$. The corresponding numbers in Weinberg's model are $b_{00}=2L\approx 0.18\mu^{-3}$, $b_{20}=-L\approx -0.09\mu^{-3}$, and $\mu^3 a_{11}=\mu^3 L/3\approx 0.03$.

V. SUMMARY AND CONCLUSIONS

We have used interior dispersion relations (IDR's) to study the $\pi\pi$ scattering amplitudes within the subthreshold region. Our conclusions are (1) that IDR's provide an excellent tool to evaluate the invariant amplitudes within the subthreshold triangle using as input data within the physical region such as scattering lengths and phase shifts. Also, in the case of $a=0$, IDR's lead naturally to the Olsson and Wanders sum rules. It was seen that the resulting amplitudes were particularly sensitive to the input parameters in the low-energy region and for various choices of input parameters did not always satisfy the expected crossing properties. (2) It was determined that all crossing properties were reasonably well satisfied if the s-wave scattering lengths a_{00} and a_{20} were correlated, i.e., lie on a ''universal curve.'' (3) The invariant amplitudes thus found are strikingly similar to the chiral-model predictions of Weinberg and others. The partial-wave amplitudes resulting from these invariant amplitudes below threshold agree with those of Pennington and Protopopescu for similar choices of a_{00} and a_{20}.

ACKNOWLEDGMENTS

We gratefully acknowledge helpful conversations with N. Fuchs, R. Jacob, and M. Scadron.

APPENDIX: DISPERSION RELATIONS FOR PWA'S AND THEIR SOLUTIONS

The partial-wave amplitude $f_{I\ell}$ and the reduced partial-wave amplitude $h_{I\ell}$ are defined by

$$f_{I\ell}\equiv(S_{I\ell}-1)/(2i\rho)\equiv\rho^{2\ell}h_{I\ell},$$

where $S_{I\ell}$ is the scattering matrix.

According to the Mandelstam representation, reduced partial-wave amplitudes have a left- and right-hand cut and satisfy a dispersion relation [25]. In its once-subtracted form,

$$f_{I\ell}=f_{I\ell}(s=0)+\frac{s}{\pi}\int_{-\infty}^{0}\frac{ds' f_{I\ell}/s'}{s'-s}+\frac{s}{\pi}\int_{\Sigma}^{\infty}\frac{ds' f_{I\ell}/s'}{s'-s}. \tag{A1}$$

If the variable s is replaced by $\rho=(1-\Sigma/s)^{1/2}$, the right-hand cut corresponds to $0\leqslant\rho\leqslant 1$ and the left-hand cut to $1\leqslant\rho\leqslant\infty$, yielding a single dispersion integral:

$$f_{I\ell}(\rho)-f_{I\ell}(\infty)=\frac{1}{\pi}\int_0^\infty\frac{d\rho'^2}{\rho'^2-\rho^2}f_{I\ell}(\rho'). \tag{A2}$$

This form is particularly attractive, since it says that functions that satisfy dispersion relations in ρ are also solutions of the original dispersion relation in s.

To illustrate the importance of this result, consider the simple one-resonance parametrization for the $\ell=0$ amplitude:

$$f_{I0}^{-1}=-i\rho+c_0+c_2\rho^2. \tag{A3}$$

The real constants c_0 and c_2 are given by the condition that the amplitude have a resonance pole at $s_r=M^2-i\Gamma M$, i.e., at $\rho=\rho_r\equiv\rho(s_r)$, $c_2=-c_0/|\rho_r|^2=(2\rho_r)^{-1}$. By writing $f_{I0}^{-1}=c_2(\rho-\rho_r)(\rho+\rho_r^*)$ it is seen that this function actually has a pair of resonance poles at ρ_r and $-\rho_r$, both located in the lower half ρ plane, i.e., unphysical s plane. The two resonance poles are complex conjugates (i.e., s_r, s_r^*) and are both on the unphysical sheet as appropriate for a resonance [26]. Thus f_{I0} is a solution of the partial-wave dispersion relation. It also satisfies elastic unitarity, $f_{I0}=\rho|f_{I0}|^2$.

Consequently, the expression for f_{I0} given by Eq. (A3) for real constants c_0 and c_2 describes a resonance, satisfies elastic unitarity, partial-wave dispersion relations, and is real analytic; i.e., it is real between its cuts. If the prescription used in Sec. II A is used to create an amplitude appropriate to describe two resonances, e.g., σ and f_0, the resulting amplitude also has satisfies elastic unitarity, partial-wave dispersion relations, and is real analytic. The obvious shortcoming of this model for f_{I0} is that it fails to include inelastic effects.

If for $\ell\geqslant 1$ a resonance parametrization for the reduced partial-wave amplitude is assumed to have the form

$$h_l^{-1}=-i\rho^{2l+1}+c_{l0}+c_{l2}\rho^2=-i\Pi_{m=1}^{2l+1}(\rho-\rho_m),$$

where the ρ_m's are the roots of $h_l^{-1}=0$, then for h_l to be real analytic, the constants c_{l0} and c_{l2} must be real and can be found by demanding that there be a resonance pole at $\rho=\rho(s_r)$. h_l also satisfies elastic unitarity. However, it can be shown that at least one of the nonresonance poles $\rho_{m'}$ is on the physical sheet and consequently this parametrization does not satisfy the appropriate dispersion relation. For a narrow width resonance such as the ρ meson this ''satellite'' pole is far from the physical region.

A solution d_l of the subtracted dispersion relation can be found by assuming $d_l=h_l$ along the cuts. Dropping the subtraction constants to avoid a pole at $s=0$ in f_l, the solution d_l can be written as

$$d_l = i \sum_{m=1}^{2l+1} \beta_m \Big/ (\rho + \varepsilon_m \rho_m),$$

where $\rho_m^{2l}\beta_m^{-1} \equiv \Pi_{m' \neq m}(\rho_m^2 - \rho_{m'}^2)$ and $\varepsilon_m \equiv \mathrm{sgn}(\rho_m)$, $\varepsilon = +1$ for the normal $i\varepsilon$ convention. If one assumes $d_l = h_l$ only along the right-hand s cut, then

$$d_l^{(rh)} = -\sum_{m=1}^{2l+1} \beta_m \frac{h(\rho) - h(\rho_m)}{\rho^2 - \rho_m^2},$$

where

$$h(\rho) \equiv \frac{\rho}{\pi}\left[\ln\left(\frac{1+\rho}{1-\rho}\right) - i\pi\right]$$

and

$$h(\rho_m) = \frac{\rho_m}{\pi}\left[\ln\left(\frac{1+\rho_m}{1-\rho_m}\right) - i\varepsilon_m \pi\right]$$

are the Chew-Mandelstam functions. This latter form is appropriate for describing a resonance contribution to a form factor and can be easily generalized to include more resonance contributions.

[1] B. R. Martin, D. Morgan, and G. Shaw, *Pion Pion Interactions in Particle Physics* (Academic Press, London, 1976). We generally follow the conventions of this book. See also J. L. Peterson, ''The $\pi\pi$ interaction,'' CERN Report No. 77-04, 1977.

[2] G. Hite, R. Jacob, and F. Steiner, Phys. Rev. D **6**, 3333 (1973).

[3] *$\pi\pi$ Scattering*, edited by P. K. Williams and V. Hagopian, AIP Conf. Proc. No. 13 (AIP, New York, 1973).

[4] W. Hoogland *et al.*, Nucl. Phys. **B69**, 185 (1974); **B126**, 109 (1977).

[5] P. Estabrooks and A. D. Martin, Nucl. Phys. **B79**, 301 (1974); **B95**, 322 (1975).

[6] B. Hyams *et al.*, Nucl. Phys. **B64**, 134 (1973); **B100**, 205 (1975).

[7] L. Rosselet *et al.*, Phys. Rev. D **15**, 574 (1977). For the prospects of a new measurement of K_{e4}, see M. Baillargeon and P. Franzini, in ''The Second DaΦne Handbook,'' edited by L. Maiani, G. Pancheri, and N. Paver, report, 1995, p. 413 (available at http://hpteor.lnf.infn.it/dafne.html).

[8] P. Estabrooks *et al.*, in *$\pi\pi$ Scattering* [3], p. 37.

[9] For a recent summary of $\pi\pi$ phase-shift data see D. Počanić, in *Workshop on Chiral Dynamics: Theory and Experiment*, edited by A. Bernstein and B. Holstein (Springer-Verlag, Berlin, 1995). A critical review of earlier phase shift data is given by W. Ochs, πN Newslett. **3**, 25 (1991). A very recent analysis of the low-energy pion production data by H. Burkhardt and J. Lowe, πN Newslett. **12**, 58 (1997), gives the scattering lengths $a_{00} = 0.193 \pm 0.008\mu^{-1}$ and $a_{20} = -0.034 \pm 0.003\mu^{-1}$ using the model of M. G. Olsson and L. Turner, Phys. Rev. Lett. **20**, 1127 (1968).

[10] D. Morgan and G. Shaw, Phys. Rev. D **2**, 520 (1970); J. L. Basdevant, C. D. Froggatt, and J. L. Peterson, Nucl. Phys. **B72**, 413 (1974). See also Chap. 10 of Ref. [1].

[11] W. Kaufmann and G. Hite, Phys. Lett. B **398**, 18 (1997).

[12] This corrects an error in Kaufmann and Hite [11] where the number $-8.5\mu^2$ was given. A slightly greater portion of the subthreshold triangle is thus available than was claimed in that article. The relationship between a (<0) and the laboratory scattering angle is $\cos\theta_L = 1/(1+\Sigma/|a|)^{1/2}$, and so for $a = -12.4\mu^2$, $\theta_L \approx 29.6°$.

[13] G. E. Hite and R. J. Jacob, Phys. Rev. D **5**, 422 (1972).

[14] G. Wanders, Helv. Phys. Acta **39**, 228 (1966).

[15] S. Weinberg, Phys. Rev. Lett. **17**, 616 (1966).

[16] N. Törnqvist and M. Roos, Phys. Rev. Lett. **76**, 1575 (1996); N. Törnqvist, Z. Phys. C **68**, 647 (1995).

[17] G. Chew and S. Mandelstam, Phys. Rev. **119**, 467 (1960). See also Ref. [1].

[18] J. Gasser and H. Leutwyler, Nucl. Phys. **B250**, 465 (1985); Phys. Lett. **125B**, 325 (1993).

[19] J. Gasser and Ulf-G. Meißner, Phys. Lett. B **258**, 219 (1991).

[20] M. Knecht, B. Moussallam, J. Stern, and N. Fuchs, Nucl. Phys. **B457**, 513 (1995).

[21] M. Knecht, B. Moussallam, and J. Stern, in ''The Second DaΦne Handbook,'' edited by L. Maiani, G. Pancheri, and N. Paver, report, 1995, p. 221.

[22] This theorem and an extensive collection of other exact results for pion-pion scattering are contained in S. M. Roy, Helv. Phys. Acta **63**, 627 (1990).

[23] M. R. Pennington and S. D. Protopopescu, Phys. Rev. D **7**, 1429 (1973). See in particular their Figs. 6 and 9.

[24] S. M. Roy, Phys. Lett. **36B**, 353 (1971).

[25] See Ref. [1], p. 233, Eq. (9.1.2).

[26] R. H. Dalitz and G. Rajasekaran, Phys. Lett. **7**, 373 (1963).